

Structure and stability of the high-pressure phase, $\text{Ca}_3\text{TiSi}_2(\text{Al,Ti,Si})_3\text{O}_{14}$

PETRA SCHEUERMANN, ALI KUTOGLU, MICHAEL SCHOSNIG,* AND EDGAR HOFFER

Department of Earth Sciences at the Philipps University, Marburg, Hans Meerweinstrasse, 35032 Marburg, Germany

ABSTRACT

The pressure and compositional dependence of element partitioning were examined in the pseudo-ternary section anorthite-titanite-perovskite of the system $\text{CaO-Al}_2\text{O}_3\text{-TiO}_2\text{-SiO}_2$. Preliminary phase relations in that section were experimentally determined at pressures from 1 atm to 1.5 GPa and at temperatures from 1300 to 1500 °C, using a double-ellipsoid mirror furnace and a piston cylinder apparatus. Further experiments were carried out with trace element extended compositions. All run products represent near-equilibrium parageneses consisting of crystals with their coexisting melt; the pairing is desired for element partitioning studies. At pressures above 1.0 GPa a new Ti-rich compound, having the ideal formula $\text{Ca}_3\text{TiSi}_2(\text{Al,Ti,Si})_3\text{O}_{14}$, appears as the dominant phase in this paragenesis.

The composition and homogeneity of the phases were checked with electron microprobe and scanning electron microscopy. Determination of the structure of this compound was performed with a conventional four circle diffractometer on a single crystal, cut from a larger specimen of the equilibrium paragenesis. The compound crystallizes in space group $P321$ with cell dimensions $a = 7.943(1)$ Å and $c = 4.930(1)$ Å. Its structure consists of layers stacked parallel to (001) such that sheets of two types of corner-linked tetrahedra (T1 = Si; T2 = Al, Ti, Si) at $z = 1/2$ alternate with sheets centered at $z = 0$ containing ^{16}Ti - and irregular eightfold-coordinated Ca-sites. A statistical distribution for Al, Si, and Ti atoms at one of the two tetrahedral sites in the crystal structure was confirmed by X-ray diffraction data. The Ti-octahedron is distorted, with $\text{Ti-O} = 1.952(3)$ Å and O-Ti-O bond angles between 85.5° and 102.4°, which results in an angle bend of the vertex O atoms of 167.6°.

INTRODUCTION

The system $\text{CaO-Al}_2\text{O}_3\text{-TiO}_2\text{-SiO}_2$ includes in its TiO_2 -rich part the stability fields of titanite (CaTiSiO_5) and perovskite (CaTiO_3). These minerals are potential hosts for the rare earth elements (REE) or the high field strength elements (HFSE: e.g., Nb, Ta, Zr, Hf), which are relevant for geochemical modeling (Green and Pearson 1986; Wooley et al. 1992; Haggerty 1983; Simon et al. 1994). Although titanite and perovskite are common accessory phases in a large number of rock types (Fleischer 1978; Hellman and Green 1979; Mitchell and Reed 1988; Onuma et al. 1981; Dawson et al. 1994), scant knowledge exists of the processes controlling element partitioning between these minerals and silicate liquid.

For this reason, we started a systematic study of the pressure and compositional dependencies of trace element partitioning between titanite-melt and perovskite-melt in the pressure range from 1 atm up to 1.5 GPa. As the starting-point of our study, we chose the pseudo-eutectic system anorthite-titanite, which has first been investigated by Prince (1943) under atmospheric pressure conditions. Schosnig (1996) stated the occurrence of perovskite at 1 atm in the course of trace element extended experiments in that system. Further studies of that system under high-pressure conditions with trace element ex-

tended compositions have first been performed by Scheuermann (1998). The results of the element partitioning studies will be reported elsewhere. During these high-pressure experiments, a new compound with composition close to $\text{Ca}_3\text{TiSi}_2(\text{Al,Ti,Si})_3\text{O}_{14}$ was discovered.

Run products of experimental studies, especially of high-pressure experiments, often possess very small crystal sizes, which are difficult to analyze or to separate (Gasparik et al. 1995; Kudoh and Kanzaki 1998; Taura et al. 1998). We present a method to obtain run products, which show near-equilibrium parageneses of crystals with coexisting melt, in which the crystals reach sizes up to 2 mm. Therefore, all analytical data could be obtained directly from polished thin sections with up to 80 data points in each single phase and from separated crystals of the new compound for structure determination, respectively.

The new phase described in this paper belongs to the structure-type with the general formula $^{18}\text{A}_x^{16}\text{B}_y^{14}\text{T}_z\text{O}_{14}$, which is also known for some synthetic germanates (Belokoneva and Belov 1981; Mill et al. 1982). Materials with this type of structure are countered to be of interest for many technological purposes, especially laser techniques (Kaminskii et al. 1984a, 1984b). Recently, Gasparik et al. (1995) described a silicate with the formula $\text{Na}_{1.8}\text{Ca}_{1.1}\text{Si}_6\text{O}_{14}$, which is isotopic to the germanates mentioned above. This silicate was discovered in high-pressure experiments between 8 and 15 GPa, whereas the $\text{Ca}_3\text{TiSi}_2(\text{Al,Ti,Si})_3\text{O}_{14}$ compound crystallizes at significantly

*E-mail: schosnig@mail.uni-marburg.de

lower pressures. To elucidate the stability field of this compound, additional experiments were carried out with stoichiometric compositions at atmospheric conditions. The structure and the presently known region of stability of $\text{Ca}_3\text{TiSi}_2(\text{Al,Ti,Si})_3\text{O}_{14}$ are presented here.

EXPERIMENTAL PROCEDURE

Experiments at 1.0 and 1.5 GPa were performed in a 1/2" diameter piston-cylinder apparatus. The 1 atm experiments were carried out using a double ellipsoid mirror furnace. In all experiments, the starting materials were mixtures of $\text{Ca}_2\text{Al}_2\text{Si}_2\text{O}_8$ and CaTiSiO_5 , synthesized from high-purity carbonates and oxides for 1 week at 1300 °C. For the trace element bearing runs, 0.5 wt% of some rare earth elements (REE_2O_3) as well as SrO and Y_2O_3 were added.

The sample assembly used in the piston-cylinder experiments consists of a double-capsule with the outer capsule containing a mixture of WO_3 and WO_2 as oxygen-buffer (length = 12 mm, diameter = 4 mm) and an inner sample-capsule (length = 9 mm, diameter = 3 mm). Each capsule was sealed by welding. The samples were put into a cylindrical graphite heater surrounded by fired pyrophyllite as the pressure medium. Temperature was measured with a Pt/PtRh thermocouple and controlled with a Eurotherm temperature controller. Pressure at the sample was calibrated as a function of oil pressure using the melting curves of CsCl and Au at 1.5 GPa. The sample capsule was located slightly off center in the assembly, so that each sample documents a temperature gradient of about 40 °C. This arrangement allows the vertical gradient freeze method, described for 1 atm in Schosnig and Hoffer (1998). As previously stated, such samples also give insight into the phase relations (Gasparik et al. 1994).

All high P experiments were performed as follows: after compressing the sample at room temperature over 12 h, the experiments were started by increasing the furnace temperature to 1450 °C within half an hour. Subsequent crystallization was initiated by reducing the temperature stepwise to the run temperature. At the run temperature, the sample was held for 3–4 h. Due to the temperature gradient in the furnace, seeding starts at the "cold" end of the sample and the crystals grow along the gradient into the "hot zone" of the furnace. At the end of the experiment, the samples were isobarically quenched by turning off the electrical power. Details are given in Scheuermann (1998).

Additional runs at atmospheric pressure conditions were performed in a double ellipsoid mirror furnace with two 2 kW halogen lamps as the heating source. A PtAu crucible (length = 10 mm, diameter = 8 mm) was used as sample container, which is attached to a corundum rod. This corundum rod can be driven vertically into the furnace, in which the sample can directly be observed by an optical lens system during the experiment. Typical run durations were in the range of 3–7 days. Over this period, the PtAu crucible was rotated constantly around the longitudinal axis at 20 to 30 r.p.m. to support convectional flow in the melt. The end of the experiment was checked optically by the simultaneous presence of crystals and coexisting melt and was achieved by rapid quenching in water. For details of the double ellipsoid mirror furnace device and crystal growth

see Schosnig (1996) and Schosnig and Hoffer (1998).

All run products were mounted in epoxy, cut along the longitudinal axis and prepared as polished thin sections. For the X-ray diffraction analyses, specific crystals of the paragenesis were separated from the thin sections.

CHEMICAL ANALYSIS

The samples were routinely checked for homogeneity by element mappings (Fig. 1) using scanning electron microscope (SEM: CamScan IV with a Noran EDX system) as well as by quantitative analyses using compositional profiles performed with electron microprobe (EMP: Cameca SX 50). Accelerating voltage for SEM was 30 kV with a resolution for the scanned area of 1024×1024 pixels and a dwell time of 0.5 ms. Quantitative analyses with EMP were performed with 25 kV accelerating voltage and an electron beam current of 40 nA. Counting time for major elements was 20 s on peak and 10 s on each background; for trace elements 40 s and 20 s respectively was chosen. Major and trace elements were measured together in one single analytical run. The analytical standards we used were mineral standards as well as glass standards especially for calibration of the trace elements as outlined further in detail in Schosnig (1996). To exclude interferences during EMP analyses the trace element bearing mixtures were split into different groups following Drake and Weill (1972).

EXPERIMENTAL RESULTS

From the different trace element bearing runs at 1.5 GPa we obtained some $^{181}\text{A}_x^{16}\text{B}_y^{14}\text{T}_z\text{O}_{14}$ equivalents containing minor amounts of trace elements. Table 1 summarizes the compositions as analyzed with EMP. The $\text{Ca}_3\text{TiSi}_2(\text{Al,Ti,Si})_3\text{O}_{14}$ formed spear-shaped crystals, 0.2 mm wide and up to 1 mm long. Light optical observations characterize the new compound as optical uniaxial positive, with a birefringence of 0.04. The optical orientation is $Z \parallel c$ with $I = +$.

All $^{181}\text{A}_x^{16}\text{B}_y^{14}\text{T}_z\text{O}_{14}$ equivalents of the 1.5 GPa runs crystallized in parageneses with anorthite, titanite, and perovskite from the melt. This is in contrast to the results of the 1.0 GPa runs, where only anorthite, titanite, perovskite, and melt coexist. The different phases can clearly be recognized by SEM element mappings as mentioned above (Fig. 1). In all cases, no zonation within the minerals or oversaturated boundary layers along phase boundaries were observed. As the chemical homogeneity is often considered as an indicator for near-equilibrium conditions (Tsuchiyama 1985; Paterson and Stephens 1992; Adam and Green 1994), the parageneses developed from both atmospheric and high-pressure runs can be regarded to be near equilibrium. We emphasize that the different phases in all experimental run products do not show any modifications of quenching and the melt is preserved as transparent glass.

To obtain more information about the stability of the $\text{Ca}_3\text{TiSi}_2(\text{Al,Ti,Si})_3\text{O}_{14}$ compound, a sample corresponding to its stoichiometric composition was prepared. The double ellipsoid mirror furnace experiments under atmospheric conditions resulted in a large intergrowth of anorthite and perovskite, indicating the simultaneous crystallization of these compounds from a melt of the ideal $\text{Ca}_3\text{TiSi}_2(\text{Al,Ti,Si})_3\text{O}_{14}$ composition.

All experiments in the system anorthite-titanite-perovskite in

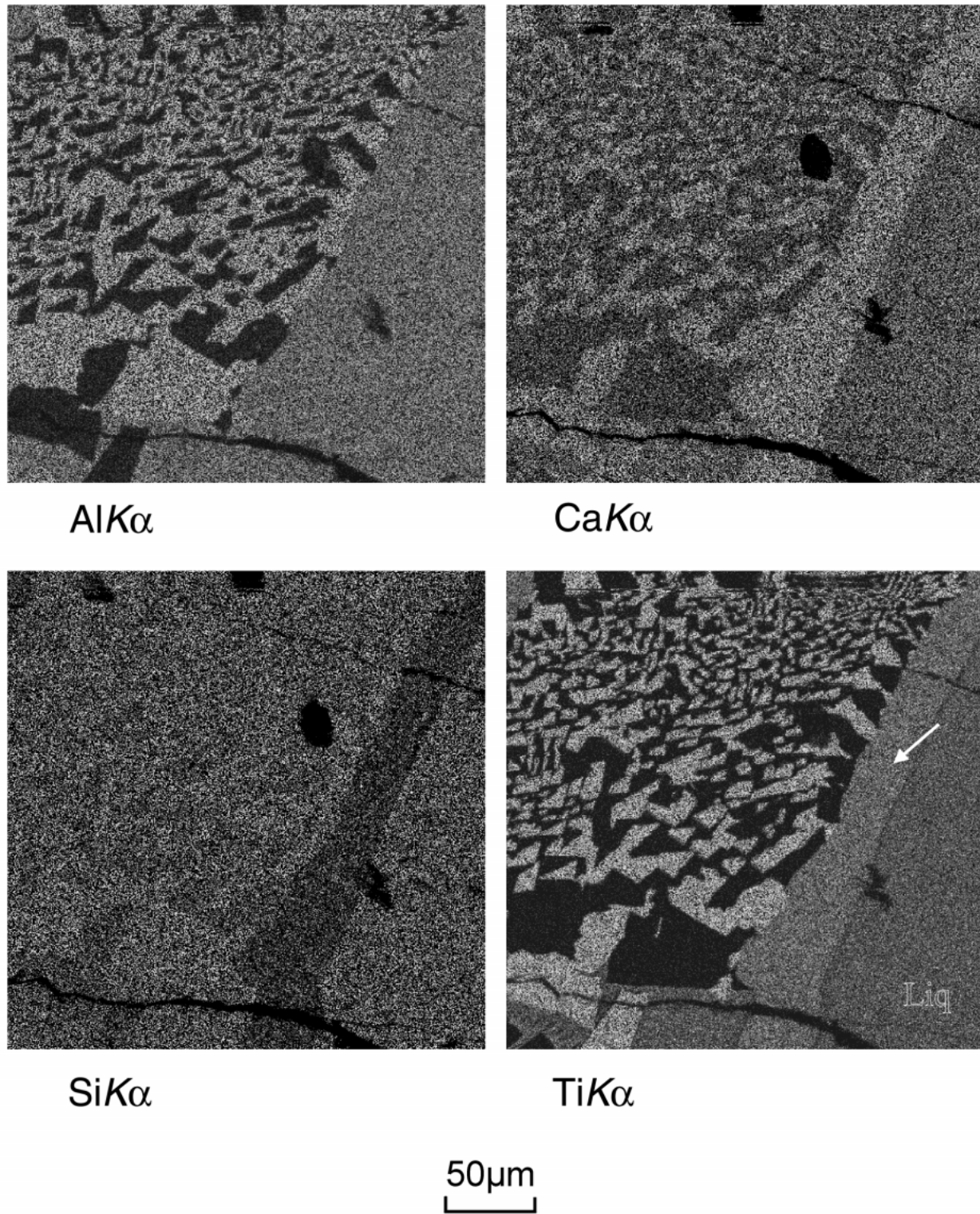


FIGURE 1. EDX-element distribution images for $\text{AlK}\alpha$, $\text{CaK}\alpha$, $\text{SiK}\alpha$, and $\text{TiK}\alpha$ lines of a quenched sample from a run at 1.5 GPa. The run product shows graphic intergrowths of anorthite, titanite, and of the quenched melt (Liq). The $\text{Ca}_3\text{TiSi}_2(\text{Al,Ti,Si})_3\text{O}_{14}$ compound is indicated by an arrow in the $\text{TiK}\alpha$ image.

TABLE 1. Chemical composition (wt%) of run products as analysed with electron microprobe

Phase	SiO ₂	TiO ₂	Al ₂ O ₃	Eu ₂ O ₃	Gd ₂ O ₃	SrO	CaO	Total
Liquid	37.0	18.4	18.0	0.5	0.5	1.2	23.2	98.8
Anorthite	43.3	0.4	35.8	0.1	0.0	1.2	19.1	99.9
Titanite	29.2	38.3	1.6	1.2	1.3	0.3	27.3	99.2
$\text{Ca}_3\text{TiSi}_2(\text{Al}, \text{Si}, \text{Ti})_3\text{O}_{14}$	26.5	22.5	18.2	0.5	0.6	0.8	29.5	98.6

TABLE 2. Crystal data and experimental details for $\text{Ca}_3\text{TiSi}_2(\text{Al},\text{Ti},\text{Si})_3\text{O}_{14}$

Space group	$D_3^3 - P321$	λ (MoK α) (Å)	0.71073
<i>a</i> (Å)	7.943(1)	no. collected refl.	3596
<i>c</i> (Å)	4.930(1)	no. unique refl.	562
<i>V</i> (Å ³)	269.4(1)	no. observed refl. [$I > 3\sigma(I)$]	458
<i>Z</i>	2	<i>R</i> / <i>R</i> _w , all	0.0312/0.0222
<i>T</i> (K)	298	<i>R</i> / <i>R</i> _w , observed	0.0180/0.0210
MW	540.27	$R = \Sigma(F_o - F_c) / \Sigma(F_o)$	$R_w = [\Sigma w(F_o - F_c)^2 / \Sigma w F_o ^2]^{1/2}$
ρ (calc) g·cm ⁻³	4.01		
μ (cm ⁻¹)	57.46	GoF	1.03

the pressure range from 1 atm up to 1.0 GPa gave no hint of $\text{Ca}_3\text{TiSi}_2(\text{Al},\text{Ti},\text{Si})_3\text{O}_{14}$ compound being stable, whereas at 1.5 GPa the crystallization of large and homogeneous $\text{Ca}_3\text{TiSi}_2(\text{Al},\text{Ti},\text{Si})_3\text{O}_{14}$ crystals takes place.

SINGLE-CRYSTAL DIFFRACTION

The structure of the new compound was determined from an irregular-shaped fragment of a colorless single crystal with maximum dimensions $0.80 \times 0.30 \times 0.20$ mm. This crystal was separated from a trace element (Sr, Eu, Gd) extended sample. The diffraction data were collected at room temperature using a Philips PW1100 four-circle diffractometer with graphite-monochromatized MoK α -radiation. Unit-cell parameters were determined by a vector least-squares calculation on 26 reflections (eight equivalent positions centering) in the range $13^\circ < 2\theta < 34^\circ$, which resulted in $a = 7.943(1)$ Å and $c = 4.930(1)$ Å for the trigonal crystal. We collected 3596 integrated intensities using the $\omega/2\theta$ scan-mode to $2\theta = 60^\circ$ ($-9 < h < 9$, $-9 < k < 9$, $0 < l < 8$). Within the collected reflections no systematic extinctions were observed. Three standard reflections chosen from different regions of the reciprocal space were monitored every 100 reflections as a check of crystal alignment and electronic fluctuations. The measured reflections were merged in pointgroup 32, resulting in a set of 562 unique reflections. The intensities were corrected for Lorentz and polarization effects, whereas an appropriate correction of absorption and extinction effects was not possible due to the irregular shape of the crystal. Standard deviations were those based on variances of the measured intensities. Structure refinements confirmed $P321$ to be the correct space group of $\text{Ca}_3\text{TiSi}_2(\text{Al},\text{Ti},\text{Si})_3\text{O}_{14}$. Our data describing the unit-cell dimensions and space group for this compound are in accordance with earlier published findings of isotopic $^{18}\text{A}_x^{16}\text{B}_y^{14}\text{T}_z\text{O}_{14}$ structures by Gasparik et al. (1995), Kaminskii et al. (1984a, 1984b), and others.

Full matrix least-squares refinements on F^2 s were carried out with the program package CRYMIS (Kutoglu 1995), applying a linear scaling factor and anisotropic displacement parameters for all atoms. Reflections for which $I < 3\sigma(I)$ were considered as unobserved and were therefore not included in the refinements. Atomic scattering factors and anomalous dispersion coefficients were taken from International Tables for Crystallography, Vol. C (Wilson 1992). Refinement details are summarized in Tables 2, 3, and 4.

According to the results of chemical analysis, the cation content composition within the structure (constrained to 14 O atoms) is Ca = 2.91, Si = 2.45, Ti = 1.56, Al = 1.98, Sr = 0.04, Eu = 0.02, and Gd = 0.02 (Table 5). Within the expected accuracy of the analytical results, we obtained only for Al an integer number, indicating uniform site occupation by this cation, whereas the values for Ca, Si, and Ti point to order-disorder type arrangements in the structure. No indications have been found for any cationic ordering on Weissenberg photographs with exposure times of 20 h. For the case of Ca and the trace elements Sr, Eu, and Gd (trace elements abbreviated by "TRE"), we assumed an analogous disordered site occupation to that formulated for Na and Ca in the structure of the high-pressure silicate $\text{Na}_{1.8}\text{Ca}_{1.1}\text{Si}_6\text{O}_{14}$ by Gasparik et al. (1995).

The structure of $\text{Ca}_3\text{TiSi}_2(\text{Al},\text{Ti},\text{Si})_3\text{O}_{14}$ is isotopic to few compounds such as the high pressure silicate $\text{Na}_{1.8}\text{Ca}_{1.1}\text{Si}_6\text{O}_{14}$ (Gasparik et al. 1995), gallo-germanates of type $\text{Me}_3\text{Ga}_2\text{Ge}_4\text{O}_{14}$ (Belokoneva and Belov 1981; Mill et al. 1982; Kaminskii et al. 1984a), and $\text{La}_3\text{NdGa}_{5.5}\text{Nb}_{0.5}\text{O}_{14}$ (Kaminskii et al. 1984b). However, the structure of $\text{Ca}_3\text{TiSi}_2(\text{Al},\text{Ti},\text{Si})_3\text{O}_{14}$ is more complicated to interpret than the isotopic high-pressure silicate of Gasparik et al. (1995). This is because of many different cations in $\text{Ca}_3\text{TiSi}_2(\text{Al},\text{Ti},\text{Si})_3\text{O}_{14}$ entering the same number of regular sites. Many site occupation alternatives for Al, Ti, and Si exist in the new CaAlTi-silicate, because of their ability to occupy both tetrahedral and octahedral sites. Therefore, a discussion about the polyhedral centering by these elements is manifold and more complex than for the phase $\text{Na}_{1.8}\text{Ca}_{1.1}\text{Si}_6\text{O}_{14}$.

The octahedral site is located at the origin of the unit cell (0, 0, 0) with point symmetry 32, whereas the remaining two independent tetrahedra (T1, T2) are situated at the Wyckoff positions 3f and 2d (point symmetries 2 and 3), respectively. To obtain more information indicative of a possible distribution of Al, Ti, and Si within that structure, all possible cation arrangements in the polyhedral centers were checked for their probable realization. At least five proposals for possible structures with low *R*-values and physically reasonable atomic displacement parameters were extracted. The results of least-squares refinements are summarized in Table 5. The octahedral site at the origin could be occupied exclusively by Ti (case 1 and 2), contemporaneously by Si and Ti (case 3 and 4) or by Al and Ti (case 5). One of the tetrahedral sites (T1 at 1/3, 2/3, *z*) can only be centered by Si or Al, but not by Ti. The

TABLE 3. Fractional atomic coordinates and equivalent isotropic displacement parameters (\AA^2) for $\text{Ca}_3\text{TiSi}_2(\text{Al,Ti,Si})_3\text{O}_{14}$ in space group $P321$

Atom	Multiplicity	Wyckoff letter	x	y	z	B_{eq}
T1	2	d	1/3	2/3	0.4631(2)	0.59(2)
T2	3	f	0.7586(2)	0	1/2	0.92(5)
Ti	1	a	0	0	0	1.16(3)
Ca	3	e	0.4240(1)	0	0	0.99(2)
O1	6	g	0.6866(4)	0.1557(3)	0.6716(4)	1.01(6)
O2	6	g	0.2230(4)	0.0849(4)	0.2413(5)	1.78(8)
O3	2	d	1/3	2/3	0.7879(7)	1.01(8)

Note: $B_{\text{eq}} = (8\pi^2/3) \cdot \sum_j \sum_k U_j a_j^* a_k^* a_j a_k$, T1 = Si, T2 = $\text{Al}_{2/3} \text{Si}_{1/6} \text{Ti}_{1/6}$ (case 1 of Table 5).

TABLE 4. Anisotropic displacement parameters for $\text{Ca}_3\text{TiSi}_2(\text{Al,Ti,Si})_3\text{O}_{14}$

Atom	U_{11}	U_{22}	U_{33}	U_{12}	U_{13}	U_{23}
T1	0.0081(4)	U_{11}	0.0062(3)	$1/2 U_{11}$	0	0
T2	0.0149(8)	0.0108(8)	0.0079(7)	$1/2 U_{22}$	$1/2 U_{23}$	0.0011(6)
Ti	0.0160(5)	U_{11}	0.0122(5)	$1/2 U_{11}$	0	0
Ca	0.0131(3)	0.0140(4)	0.0110(3)	$1/2 U_{22}$	$1/2 U_{23}$	0.0001(2)
O1	0.0156(10)	0.0132(7)	0.0109(8)	0.0082(8)	0.0025(6)	0.0012(6)
O2	0.0222(11)	0.0266(14)	0.0231(9)	0.0154(10)	-0.0077(8)	-0.0075(9)
O3	0.0154(14)	U_{11}	0.0077(13)	$1/2 U_{11}$	0.0	0.0

Note: $\text{Exp}\{2\pi^2[U_{11}h^2a^2 + 2(U_{12}hka^*b^* \dots)]\}$.

TABLE 5. Possible cation arrangements in the crystal structure of $\text{Ca}_3\text{TiSi}_2(\text{Al,Ti,Si})_3\text{O}_{14}$

Site	1	2	3	4	5
T1	Si	Al	Al	Si	Si
a	2.0	2.0	2.0	2.0	2.0
b	2.0	2.0	2.0	2.0	2.0
T2	Al / Si / Ti	Si / Ti	Si / Ti	Al / Ti	Al / Si / Ti
a	2.0 / 0.5 / 0.5	2.76 / 0.24	2.88 / 0.12	2.51 / 0.49	1.97 / 0.59 / 0.43
b	2.0 / 0.44 / 0.56	2.72 / 0.28	2.81 / 0.19	2.45 / 0.55	2.11 / 0.38 / 0.50
Oct	Ti	Ti	Ti / Si	Ti / Si	Ti / Al
a	1.0	1.0	0.83 / 0.17	0.91 / 0.9	0.99 / 0.01
b	1.0	1.0	0.85 / 0.15	0.94 / 0.06	0.94 / 0.06
Ca/TRE	Ca / TRE	Ca / TRE	Ca / TRE	Ca / TRE	Ca / TRE
a	2.94 / 0.06	2.97 / 0.03	3.03 / -0.03	2.96 / 0.04	3.00 / 0.00
b	2.90 / 0.10	2.94 / 0.06	2.98 / 0.02	2.91 / 0.09	2.74 / 0.26
$R_{\text{iso}} / R_{\text{aniso}}$	3.83 / 1.81	3.86 / 1.94	3.78 / 1.81	3.83 / 1.80	3.83 / 1.87

Cation compositions revealed by EMP analyses constrained to 14 O atoms and results of least-squares calculations for cases 1–5

EMP	1		2		3		4		5		
	a	b	a	b	a	b	a	b	a	b	
Ti ⁴⁺	1.56	1.50	1.56	1.24	1.28	0.95	1.04	1.40	1.49	1.35	1.44
Si ⁴⁺	2.45	2.50	2.44	2.76	2.72	3.05	2.96	2.09	2.06	2.59	2.38
Al ³⁺	1.98	2.00	2.00	2.00	2.00	2.00	2.00	2.51	2.45	1.97	2.17
Ca ²⁺	2.91	2.94	2.90	2.97	2.94	3.03	2.90	2.96	2.91	3.00	2.74
TRE ^{2+/3+}	0.08	0.06	0.10	0.03	0.06	-0.03	0.02	0.04	0.09	0.00	0.26

Notes: a = isotropic displacement parameters; b = anisotropic displacement parameters. Data in the lower part refer to cation numbers in the unit cell.

remaining tetrahedron T2 (at x, 0, 0) is to be occupied either by Si together with Ti (case 2 and 3) or by Al in common with Ti (case 4) or by Al, Si, and Ti (case 1 and 5).

A comparison of the numbers of atoms for Al, Ti, and Si resulting from least-squares calculations with those determined by electron microprobe analyses reveals large discrepancies for the cases 2, 3, 4, and 5 (Table 5), but there is an excellent agreement between the results of the isotropic and anisotropic refinements for case 1.

In accord with these primary calculations and the results given by microprobe analysis, terminal least-squares refinements were carried out for the compositional formula $(\text{Ca}_{3-x}\text{TRE}_x)\text{TiSi}_2(\text{Al}_{2-x}\text{Ti}_{1-x}\text{Si}_x)\text{O}_{14}$ with $x = 0.08$ and $y = 0.45$. Within the refinements, one half of x was fixed to represent the amount of Sr and the second one that of Eu and Gd "impurities." With respect to the site occupation

parameter at T2 and ascertainments by electron microprobe analyses, we constrained $2/3$ of the T2 site to be occupied by Al and the remaining $1/3$ by Si and Ti in proportions given by the y-value. The final positional and anisotropic displacement parameters are given in Table 3 and 4. Geometrical descriptions of the coordination polyhedra are reported in Table 6.

Small amounts of any other mutual replacements of Al, Si, and Ti atoms are possible, which cannot be detected by X-ray diffraction methods. This aspect will be discussed later.

DISCUSSION

A consequence of several sites being occupied by different cations is a distortion of the polyhedra, which depends on the type of these central atoms. Especially in cases where the coordination polyhedra are distorted, bond-strength bond-length

relationships (Pauling 1929; Brown and Shannon 1973) are a useful tool in accounting for bonding. If a crystal structure is accurately determined and the cation-anion distances are comparable with those expected, the sums of bond strength around the cations and anions, respectively, should be equal to their valences. The structure of $\text{Ca}_3\text{TiSi}_2(\text{Al,Ti,Si})_3\text{O}_{14}$ contains two independent tetrahedra with different central cations, an octahedron, and an irregular polyhedron. Hence, this structure should be an excellent test of the above relationship.

Description of the structure

The main structural elements of $\text{Ca}_3\text{TiSi}_2(\text{Al,Ti,Si})_3\text{O}_{14}$ are two different layers parallel (001) as can be seen in Figure 2. One of these is a layer at $z = 1/2$ consisting of two symmetrically distinct corner-linked tetrahedra (T1, T2), centered exclusively by Si (T1) or by a combination of Al, Ti, and Si (T2). These tetrahedra form open-branched crankshaft vierer chains (Liebau 1985), crosslinked by individual tetrahedra. The linkage occurs along a chain alternating by three (T1) and two (T2) oxygen atoms (O1) of the tetrahedra. Those tetrahedra-sheets alternate with layers at $z = 0$ containing Ti cations, which are octahedrally coordinated by oxygen anions (O2). These oxygen anions are not involved in the tetrahedra linkage, whereas the octahedron and each tetrahedron T2 share common corners. This framework of corner-linked tetrahedra produces eightfold-coordinated sites that are mainly occupied by Ca^{2+} or by di-/trivalent trace elements Sr, Eu, and Gd.

Tetrahedron T1

The tetrahedron T1 is exclusively occupied by Si. The threefold axial symmetry at the Si and O3 sites created two distinct distances: $3 \times 1.637 \text{ \AA}$ (Si-O1) and $1 \times 1.601 \text{ \AA}$ (Si-O3) (Table 6). In comparison to the analogous distances ($3 \times 1.638 \text{ \AA}$, $1 \times 1.557 \text{ \AA}$) of the isotypic high-pressure silicate (Gasparik et al. 1995), there is an excellent agreement for the larger distance but not so for the shorter one, whereas the sum of effective ionic radii for the Si-O distance in tetrahedral coordination after Shannon (1976) amounts to 1.64 \AA .

Gasparik et al. (1995) stated a larger atomic displacement parameter for that oxygen forming this bond, but in the present structure we did not estimate a parametric anomaly giving rise to such a shortening. We assume a stronger valence bond character in the non-bridged Si-O3 bond, which finds its expression in the calculated valence sums (Brown and Shannon 1973) for O1, O2, and O3 (1.97, 1.93, and 1.64).

Another aspect concerning tetrahedron T1 is the degree of distortion from holosymmetric geometry. Various criteria can be used to describe polyhedral distortion, from which a reliable method for a quantitative measure is given by Robinson et al. (1971) using quadratic elongation and bond angle variance. Applying this formalism to the T1-tetrahedron of $\text{Ca}_3\text{TiSi}_2(\text{Al,Ti,Si})_3\text{O}_{14}$, we obtained the values 1.006 for quadratic elongation and 25.8° angular variance, indicating a moderate polyhedral distortion.

Tetrahedron T2

A larger differentiation exists within the second tetrahedron (T2), which is occupied by Al, Si, and Ti. Because of the two fold axial symmetry, the calculated T2-O bond distances are pairwise 1.735 \AA and 1.811 \AA (average 1.773 \AA). These values differ considerably from those in T1, reflecting the complex behavior defined by the cationic site occupation by Al^{3+} , Ti^{4+} , and Si^{4+} . The dominant cation in T2 is Al, so we expect a bond distance closer to that of the pure Al-O distance. Based on the effective ionic radii given by Shannon (1976), the Al-O, Si-O, and Ti-O distances have to be 1.77 \AA , 1.64 \AA , and 1.80 \AA . Mixing these values according to their amount given by the site occupation numbers (Table 5), we calculate a fictive T2-O bond distance of 1.757 \AA , which is smaller than the T2-O average of 1.773 \AA . This enlargement of the T2-O bond may partially be caused by positional uncertainty of the O2-site due to the elevated atomic displacement parameter (Table 4).

Inspection of the values given in Table 4 shows clearly that this tetrahedron undergoes significant distortion, indicated by divergent T2-O distances (1.735 and 1.811 \AA) as well as by a large spread within the O-T2-O bond angle values (Table 6). Five of them have the values 97.8° to 106.4° , whereas the last

TABLE 6. Relevant interatomic distances (\AA) and angles ($^\circ$) for $\text{Ca}_3\text{TiSi}_2(\text{Al,Si,Ti})_3\text{O}_{14}$

Atoms	Dist/ang.	Atoms	Angles
T1-O1	1.637(2) $\times 3$	O2-Ti-O2	85.5(1) $\times 3$
T1-O2	1.601(2)	O2-Ti-O2	86.7(1) $\times 6$
mean T1-O	1.628	O2-Ti-O2	102.4(1) $\times 3$
		O2-Ti-O2	167.6(1) $\times 3$
T2-O2	1.735(3) $\times 2$	O1-Ca-O1	58.30(7) $\times 2$
T2-O1	1.811(3) $\times 2$	O1-Ca-O3	68.33(6) $\times 2$
mean T2-O	1.773	O2-Ca-O3	68.84(10)
Ti-O2	1.952(3) $\times 6$	O1-Ca-O2	69.04(9) $\times 2$
		O1-Ca-O3	74.85(7) $\times 2$
Ca-O2	2.345(3) $\times 2$	O2-Ca-O3	76.53(8) $\times 2$
Ca-O1	2.433(2) $\times 2$	O1-Ca-O2	80.94(9) $\times 2$
Ca-O3	2.591(2) $\times 2$	O1-Ca-O3	88.88(7) $\times 2$
Ca-O1	2.838(2) $\times 2$	O1-Ca-O2	105.63(9) $\times 2$
		O1-Ca-O1	105.83(8)
O1-T1-O1	104.7(1) $\times 3$	O1-Ca-O3	120.93(7) $\times 2$
O1-T1-O3	113.9(1) $\times 3$	O2-Ca-O3	128.12(9) $\times 2$
		O1-Ca-O2	136.50(9) $\times 2$
O1-T2-O1	97.8(1)	O1-Ca-O1	143.62(7)
O1-T2-O2	104.1(1) $\times 2$	O3-Ca-O3	153.06(6)
O1-T2-O2	106.4(1) $\times 2$	O1-Ca-O1	154.45(8) $\times 2$
O2-T2-O2	132.8(1)	T1-O1-T2	126.8(1)

Note: Identical atom numbers may refer to different symmetry operations.

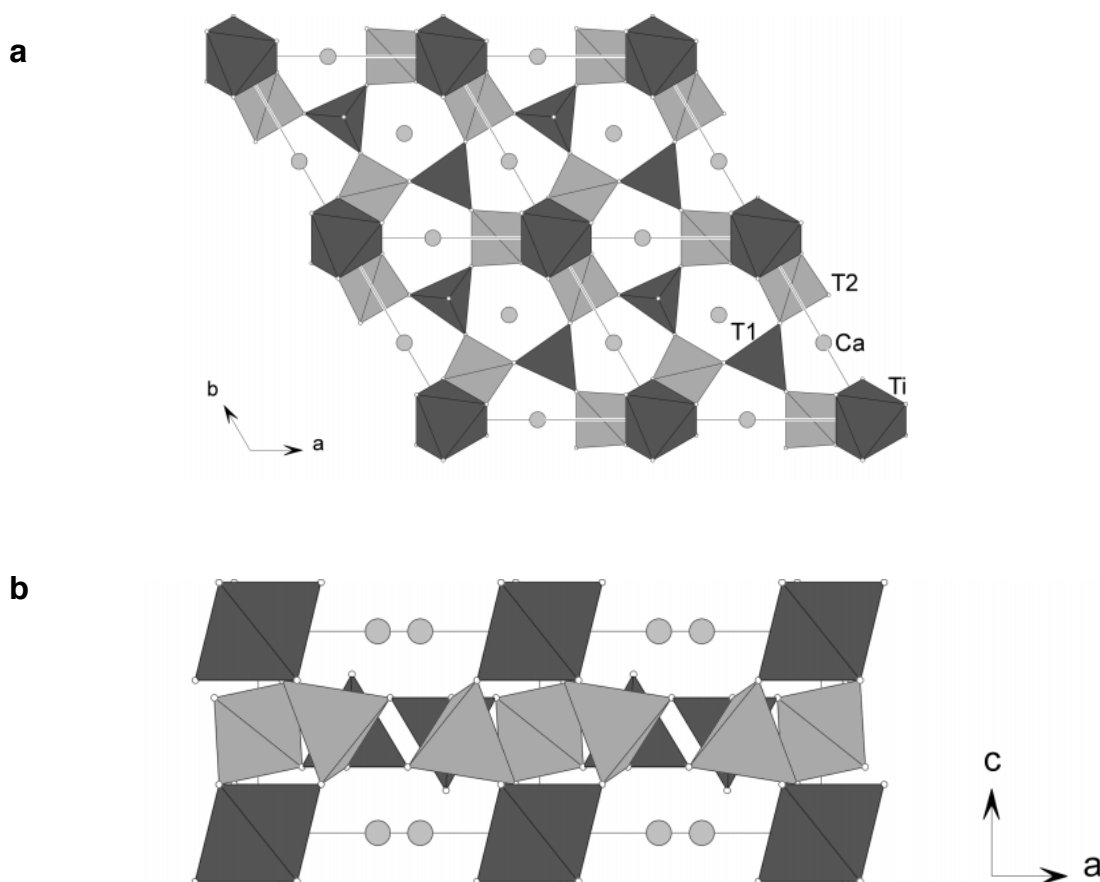


FIGURE 2. (a) The crystal structure of $\text{Ca}_3\text{TiSi}_2(\text{Al,Ti,Si})_3\text{O}_{14}$ projected on the (001) plane. (b) Projection of the structure along the b -axial direction showing the tetrahedral layer at $z = 1/2$ and the octahedral layer containing the Ca-sites at $z = 0$. Atom labels as in Table 3.

one diverges to 132.8° . Derived quadratic elongation of 1.033 and angular variance of 151.7° reflect extended polyhedral distortion of this tetrahedron. There is no reasonable explanation for such an angular distortion even if the atomic displacement parameter of the O2 oxygen, which is exclusively involved in this bond angle, is almost twice larger than those of the other O atoms (Table 4). Similar observations were made of the isotopic high-pressure silicate $\text{Na}_{1.8}\text{Ca}_{1.1}\text{Si}_6\text{O}_{14}$ by Gasparik et al. (1995).

Ca-Polyhedron

An irregular eightfold coordination is found for Ca and the TRE. There are six shorter Ca-O distances ranging from 2.345 to 2.591 Å (Table 6) and two longer ones of 2.838 Å giving the average 2.54 Å, a value which is exactly equal to the sum of effective ionic radii of Ca and O given by Shannon (1976). This more complex polyhedral arrangement shows a wide range in angle distribution from 58.30° to 154.45° (Table 6).

Octahedron

The Ti-octahedron (Table 6) has a unique Ti-O distance of 1.952 Å, which is remarkably shorter than the sum of effective ionic radii (2.01 Å; Shannon 1976). For a comparative discussion of our data, we selected two representatives from a num-

ber of Ti-bearing crystal structures, mainly silicates with octahedrally coordinated titanium. The Ti-O distance in the crystal structure of titanite CaTiOSiO_4 (Mongiorgi and Riva di Sanseverino 1968) ranges from 1.874 Å to 2.024 Å (average 1.961 Å). Oberti et al. (1991) discuss the crystal-chemistry of high-aluminum titanite, in which octahedral Ti-O distances between 1.778 and 2.025 Å have been determined (average 1.958 Å). In the structure of rutile (TiO_2) the estimated average Ti-O distance is 1.959 Å (Baur 1956). These distances agree well with the Ti-O distance determined in the structure presented here.

Nevertheless, the octahedron is slightly distorted with O-Ti-O bond angles ranging between 85.5° and 102.4° (Table 6) instead of 90° , which has to be expected for ideal octahedral configuration. This polyhedral distortion is also clearly demonstrated by the amount of angle bend concerned to the vertex O atoms of 167.6° instead of expected 180° . For this site we calculated 53.6° angle variance and 1.016 for quadratic elongation. The same polyhedral quadratic elongation was extrapolated from the graphical construction given by Robinson et al. (1971). Using parameters for bond-strength bond-length curves for oxides given by Brown and Shannon (1973), we calculated for the tetravalent Ti the valence numbers 3.98 (universal pa-

rameters) and 4.00 (corrected for oxygen coordination).

The contraction of the octahedron might be caused by some $\text{Si} \leftrightarrow \text{Ti}$ exchange between T2 and the octahedral site, which cannot clearly be resolved by the X-ray data. For that reason we calculated distances for 1/4 Si at the octahedral site, which are expected to be $\text{M}-\text{O} = 1.95$ and $\text{T2}-\text{O} = 1.775 \text{ \AA}$. These data show good agreement with the distances determined by X-ray diffraction, but these findings should also be checked by NMR studies.

For comparison, in the isotopic high-pressure silicate of Gasparik et al. (1995) the coordination environments of Si are determined to be octahedral as well as tetrahedral at pressures between 8 and 14 GPa. As such mixed-coordination phases often occur due to coordination changes of Si from tetrahedral to octahedral with increasing pressure, the $\text{Ca}_3\text{TiSi}_2(\text{Al}, \text{Ti}, \text{Si})_3\text{O}_{14}$ phase might be a low-pressure representative with small amounts of Si substitution on the Ti octahedron. Recently, Knoche et al. (1998) reported on the substitution of ^{16}Si for ^{16}Ti in titanite and they stated that the incorporation of octahedral silicon into titanite already becomes significant at fairly low pressures of about 3.5 GPa. This indicates the relevance of octahedral silicon also at relatively low pressures. Therefore, one can suppose that the new compound belongs to a solid solution series with increasing ^{16}Si at increasing pressure.

ACKNOWLEDGMENTS

The authors thank Andreas Schaper for access to the SEM, Werner Treutmann for access to the double ellipsoid mirror furnaces, and Rüdiger Borchardt for his assistance during EMP analyses. The experiments benefited from the help of Heinz-Otto Brauer, Norbert Lessmann, and Werner Schäfer. We thank Rudolf Allmann for revision of the manuscript and helpful annotations. Rebecca A. Couillard and Kaye Savage kindly corrected earlier versions of the manuscript. Roberta Oberti, Kurt Leinenweber, and an anonymous reviewer are thanked for constructive and helpful comments.

REFERENCES CITED

- Adam, J. and Green, T.H. (1994) The effects of pressure and temperature on the partitioning of Ti, Sr, and REE between amphibole, clinopyroxene and basaltic melts. *Chemical Geology*, 117, 219–233.
- Baur, W.H. (1956) Über die Verfeinerung der Kristallstrukturbestimmung einiger Vertreter des Rutiltyps: TiO_2 , SnO_2 , GeO_2 und MgF_2 . *Acta Crystallographica*, 9, 515–520.
- Belokoneva, E.L. and Belov, N.V. (1981) The crystal structure of the synthetic Ga-Ge-gelenite $\text{Ca}_2\text{Ga}_2\text{GeO}_7$ and its comparison with the structure $\text{Ca}_3\text{Ga}_2\text{Ge}_4\text{O}_{14} = \text{Ca}_3\text{Ge}((\text{Ga}_2\text{Ge})\text{Ge}_2\text{O}_{14})$. *Doklady Akademii Nauk SSSR*, 260, 1363–1366.
- Brown, I.D. and Shannon, R.D. (1973) Empirical bond-strength-bond-length curves for oxides. *Acta Crystallographica*, A29, 266–282.
- Dawson, J.B., Smith, J.V., and Steele, I.M. (1994) Trace-element distribution between coexisting perovskite, apatite and titanite from Oldoinyo Lengai, Tanzania. *Chemical Geology*, 117, 285–290.
- Drake, M.J. and Weill, D.F. (1972) New rare earth element standards for electron microprobe analysis. *Chemical Geology*, 10, 179–181.
- Fleischer, M. (1978) Relation of the relative concentrations of lanthanides in titanite to type of host rocks. *American Mineralogist*, 63, 869–873.
- Gasparik, T., Wolf, W., and Smith, C.M. (1994) Experimental determination of phase relations in the CaSiO_3 system from 8 to 15 GPa. *American Mineralogist*, 79, 1219–1222.
- Gasparik, T., Parise, J.B., Eiben, B.A., and Hriljac, J.A. (1995) Stability and structure of a new high-pressure silicate, $\text{Na}_{18}\text{Ca}_1\text{Si}_6\text{O}_{14}$. *American Mineralogist*, 80, 1269–1276.
- Green, T.H., and Pearson, N.J. (1986) Rare-earth element partitioning between sphene and coexisting silicate liquid at high pressure and temperature. *Chemical Geology*, 55, 105–119.
- Haggerty, S.E. (1983) The mineral chemistry of new titanates from the Jagersfontein kimberlite, South Africa: Implications for metasomatism in the upper mantle. *Geochimica et Cosmochimica Acta*, 47, 1833–1854.
- Hellman, P.L. and Green, T.H. (1979) The role of sphene as an accessory phase in the high-pressure partial melting of hydrous mafic compositions. *Earth and Planetary Science Letters*, 42, 191–201.
- Kaminskii, A.A., Belokoneva, E.L., Mill, B.V., Pisarevskii, Y.V., Sarkisov, S.E., Silvestrova, I.M., Butashin, A.V., and Khodzhabagyan, G.G. (1984a) Pure and Nd^{3+} -doped $\text{Ca}_3\text{Ga}_2\text{Ge}_4\text{O}_{14}$ and $\text{Sr}_3\text{Ga}_2\text{Ge}_4\text{O}_{14}$ single crystals, their structure optical, spectral luminescence, electromechanical properties, and stimulated emission. *Physica Status Solidi, Section A: Applied Research*, 86, 345–362.
- Kaminskii, A.A., Mill, B.V., Belokoneva, E.L., Sarkisov, S.E., Pastukhova, T.Y., and Khodzhabagyan, G.G. (1984b) Crystal structure and stimulated emission of $\text{La}_3\text{Ga}_2\text{Nb}_2\text{O}_{14}$. *Izvestiya Akademii Nauk SSSR, Neorganicheskie Materialy*, 2058–2062.
- Knoche, R., Angel, R.J., Seifert, F., and Fliervoet, T.F. (1998) Complete substitution of Si for Ti in titanite $\text{Ca}(\text{Ti}_{1-x}\text{Si}_x)\text{Si}^{\text{IV}}\text{O}_5$. *American Mineralogist*, 83, 1168–1175.
- Kudoh, Y., and Kanzaki, M. (1998) Crystal chemical characteristics of α - CaSi_2O_5 , a new high pressure calcium silicate with five-coordinated silicon synthesized at 1500°C and 10 GPa. *Physics and Chemistry of Minerals*, 25, 429–433.
- Kutoglu, A. (1995) CRYMIS: A Fortran Programme System (1986) Version 1995, Internal Report. Institut für Mineralogie, Petrologie und Kristallographie. Universität Marburg, Germany.
- Liebau, F. (1985) Structural chemistry of silicates. 247 p. Springer Verlag, Berlin.
- Mill, B.V., Butashin, A.V., Khodzhabagyan, G.G., Belokoneva, E.L., and Belov, N.V. (1982) The modified rare-earth gallates with the structure of $\text{Ca}_3\text{Ga}_2\text{Ge}_4\text{O}_{14}$. *Doklady Akademii Nauk SSSR*, 1385–1389.
- Mitchell, R.H. and Reed, S.J.B. (1988) Ion microprobe determination of rare earth elements in perovskite from kimberlites and alnöites. *Mineralogical Magazine*, 52, 331–339.
- Mongiorgi, R. and Riva di Sanseverino, L. (1968) A reconsideration of the structure of titanite CaTiOSiO_4 . *Mineralogica et Petrographica Acta*, 14, 123–141.
- Oberti, R., Smith, D.C., Rossi, G., and Caucia, F. (1991) The crystal-chemistry of high-aluminium titanites. *European Journal of Mineralogy*, 3, 777–792.
- Onuma, N., Ninomiya, S., and Nagasawa, H. (1981) Mineral/groundmass partition coefficients for nepheline, melilite, clinopyroxene and perovskite in melilite-nepheline basalt, Nyiagongo, Zaire. *Geochemical Journal*, 15, 221–228.
- Paterson, B.A. and Stephens, W.E. (1992) Kinetically induced compositional zoning: implications for accessory-phase/melt partitioning of trace elements. *Contributions to Mineralogy and Petrology*, 109, 373–385.
- Pauling, L. (1929) The principles determining the structure of complex ionic crystals. *Journal of the American Chemical Society*, 51, 1010–1026.
- Prince, A.T. (1943) The system albite-anorthite-sphene. *Journal of Geology*, 51, 1–16.
- Robinson, K., Gibbs, J.V., and Ribbe, P.H. (1971) Quadratic elongation, a quantitative measure of distortion in co-ordination polyhedra. *Science*, 172, 567–570.
- Scheuermann, P. (1998) Experimentelle Untersuchungen zur Spurenelementverteilung zwischen Titanit, Perovskit und Schmelze im System Anorthit-Titanit bei 10 und 15 kbar. Diploma Thesis, Philipps-Universität Marburg.
- Schosnig, M. (1996) Experimentelle Untersuchungen im System Anorthit-Diopsid-Titanit bei Atmosphärenbedingungen. Ph.D. Thesis, Philipps-Universität Marburg.
- Schosnig, M. and Hoffer, E. (1998) Compositional dependence of REE-partitioning between diopside and melt at 1 atmosphere. *Contributions to Mineralogy and Petrology*, 133, 205–216.
- Shannon, R.D. (1976) Revised effective ionic radii and systematic studies of interatomic distances in halides and chalcogenides. *Acta Crystallographica*, A32, 751–767.
- Simon, S.B., Kuehner, S.M., Davis, A.M., Grossman, L., Johnson, M.L., and Burnett, D.S. (1994) Experimental studies of trace element partitioning in Ca, Al-rich compositions: Anorthite and perovskite. *Geochimica et Cosmochimica Acta*, 58, 1507–1523.
- Taura, H., Yurimoto, H., Kurita, K., and Sueno, S. (1998) Pressure dependence on partition coefficients for trace elements between olivine and coexisting melts. *Physics and Chemistry of Minerals*, 25, 469–484.
- Tsuyhama, A. (1985) Crystallization kinetics in the system $\text{CaMgSi}_2\text{O}_6$ - $\text{CaAl}_2\text{Si}_2\text{O}_7$: development of zoning and kinetic effects on element partitioning. *American Mineralogist*, 70, 474–486.
- Wilson, A.J.C. (1992) International Tables for Crystallography. Volume C. Kluwer Academic Publishers, Dordrecht.
- Woolley, A.R., Platt, R.G., and Eby, N. (1992) Niobian titanite and eudialyte from the Ilomba nepheline syenite complex, North Malawi. *Mineralogical Magazine*, 56, 428–430.

MANUSCRIPT RECEIVED JUNE 8, 1999

MANUSCRIPT ACCEPTED DECEMBER 17, 1999

PAPER HANDLED BY YANBIN WANG